

promoting access to White Rose research papers



Universities of Leeds, Sheffield and York
<http://eprints.whiterose.ac.uk/>

This is the author's post-print version of an article published in **Soft Matter**

White Rose Research Online URL for this paper:

<http://eprints.whiterose.ac.uk/id/eprint/78254>

Published article:

Yow, HN and Biggs, S (2013) *Probing the stability of sterically stabilized polystyrene particles by centrifugal sedimentation*. *Soft Matter*, 9 (42). 10031 - 10041. ISSN 1744-683X

<http://dx.doi.org/10.1039/c3sm51534f>

Cite this: DOI: 10.1039/c0xx00000x

www.rsc.org/xxxxxx

ARTICLE TYPE

Probing the stability of sterically-stabilized polystyrene particles by centrifugal sedimentation

Huai Nyin Yow*^a and Simon Biggs^a

Received (in XXX, XXX) Xth XXXXXXXXXX 20XX, Accepted Xth XXXXXXXXXX 20XX

DOI: 10.1039/b000000x

The stability and sedimentation behaviour of sterically-stabilized temperature-sensitive colloidal particles has been investigated as a function of temperature and electrolyte concentration via an analytical centrifugation technique, the LUMiSizer®. The technique builds a steady particle bed at low centrifugal acceleration (~145 g), that is subsequently assessed in terms of network strength as the centrifugal field is increased up to ~2325 g. Stable particle dispersions produce a smooth constant profile irrespective of applied force, whilst aggregated dispersions show a stepwise compression profile with increasing force. The extent of bed compression, which correlates to the degree of particle aggregation, is more prominent at high electrolyte concentrations and temperatures. This is due to the dehydration of the steric stabilising layer and/or electrical double layer screening effects, which induce greater instability in the particles. Equilibrium compressive yield stress, $P_y(\phi_{eq})$, has been used to characterise the bed compression responses. $P_y(\phi_{eq})$ shows a power-law dependency on the particle volume fraction, with a denser bed produced at lower electrolyte concentrations at a given centrifugal force. $P_y(\phi_{eq})$ analysis has also assisted in describing the differences in particle structure as a function of thermal stability of the colloidal particles (i.e. 'sterically-repulsive solvated polymeric shell or 'attractive' collapsed polymeric shell).

1. Introduction

Colloidal stability is vital in various industries and associated products, such as paints, inks, foodstuff, skincare, pesticides, electrophoretic displays and others. This is driven by the need to maintain consistent product properties, which can be in terms of formulation behavior (e.g. rheology, electrical response, deposition structures, etc.) and/or formulation appeal (e.g. aesthetics, texture, shelf life, etc.). Colloidal stability is governed by the interactions between particles in dispersion, as determined by the balance of the attractive van der Waals forces and any repulsive forces (e.g. electrostatic and/or steric repulsion) acting on the particles.^{1,2} Without sufficient stabilization, the particles will aggregate rapidly and this can be irreversible if any externally applied separation force (e.g. in stirring, sonication, etc.) is smaller than the attractive forces holding the aggregates together. Further aggregation can lead to separation through macroscopic sedimentation of the particles, resulting in unusable colloidal dispersions.

Colloidal stability is often an intricate balance in real systems because of the formulation complexity in commercial dispersions. Typically, these contain more than one colloidal component (e.g. organic pigments, oxide nanoparticles, polymeric thickeners, microcapsules, etc.) and include a range of other additives, such as volatile actives, electrolyte, viscosity modifier, humectant amongst others. This makes the formulation of a stable colloidal dispersion laborious and it can also be difficult to judge the colloidal stability in the early formulation stages without performing lengthy 'stability' experiments. There are two main techniques that have been generally employed to study the stability of colloidal dispersions,^{3,4,5} (i) light scattering and (ii)

turbidity measurements. Both techniques have their drawbacks: light scattering relies on the dilution of dispersions to very low concentrations, which may alter the aggregation behavior^{6,7} while turbidity measurements can take long times, particularly for systems with small particles and/or small density differences between the particles and suspending medium.⁸ Recently, an analytical multi-sample centrifugation technique, the LUMiSizer®, has been used to characterize the stability of colloidal dispersions for early formulation stability tests within shorter timescales.⁹ Reports using this accelerated characterization technique have explored the effects of electrolyte,⁹ polymer concentration^{10,11,12} and preparation techniques¹³ on the colloidal stability of a range of particles (e.g. silica,^{9,10,11} cellulose,⁹ calcium carbonate,¹⁰ organic pigments,¹³ composites,¹² etc.). Through observation of the particle front as sedimentation occurs, and the speed of this front movement, it is possible to characterize the quality of colloidal dispersions (aggregated or stable) and determine the optimum formulation and/or preparation protocol.

An extension to the analytical centrifugation technique is the characterization of particle beds formed from the step-wise application of a centrifugal force onto colloidal dispersions. This was first demonstrated by Buscall,¹⁴ who subsequently developed the theory behind compressive rheology with White.¹⁵ The compressive yield stress, $P_y(\phi)$, which is used to characterize the strength of a compressed particle bed, has been found to be dependent on the shear history during the aggregation process, the strength of inter-particle interaction forces, and the local volume concentration of particles. A review by Scales *et al.*¹⁶ has illustrated the use of compressive rheology to deduce both the compressibility and permeability of particle networks (using, for

example, latex,¹⁷ silica,¹⁸ zirconia,¹⁹ alumina,^{6,19} tailings,²⁰ etc.). It is also shown that compressive rheology correlates well with aggregate size⁶ and other rheological properties, such as shear yield stress,^{6,17} storage modulus,^{17,18} etc.

The current paper summarizes the use of a commercial analytical centrifugation technique to investigate the effects of electrolyte concentration and temperature on the stability of dispersions of a sterically-stabilized colloid. The steric stabilizer of choice here is a poly(ethylene glycol)-based polymer, which is known to be responsive to both temperature and addition of electrolytes.^{21,22} Of particular interest is the influence of inter-particle interactions between sterically-stabilized particles on the quality of the colloidal dispersions and the network strength of the particle beds formed.

2. Materials and methods

2.1. Materials

Styrene ($\geq 99\%$, Sigma-Aldrich) was vacuum distilled at 40°C before use to remove the inhibitor. The following chemicals were used as received; azobisisobutyronitrile (AIBN) (Camida Ltd), methanol ($\geq 99.9\%$, Sigma-Aldrich), ethanol (99.8+%, Fisher Scientific) and potassium chloride (KCl) ($\geq 99\%$, Sigma-Aldrich). The polymeric stabilizer, methoxypolyethylene glycol methacrylate (PEGMA) with molecular weight (MW) ~ 2080 g/mol, was kindly donated by IMCD UK Ltd as 50% aqueous solution and used as received. 10 and 100 mM hydrochloric acid (HCl) (32%, Sigma-Aldrich) and potassium hydroxide (KOH) (90+%, Sigma-Aldrich) solutions were used to adjust the pH of the samples when required. Millipore water (18.2 M Ω .cm) was used in all sample preparation.

2.2. Particle dispersion synthesis

The sterically-stabilized polystyrene particles were synthesized in-house according to the method of Fujii *et al.*²³ The procedures are described briefly in the following. 45.0 mL methanol and 4.75 mL Millipore water were added into a 100 mL three-neck round-bottom flask. 0.50 g PEGMA stabilizer was stirred with a magnetic stirrer bar into 90:10 (v/v) methanol/water. The mixture was degassed with nitrogen gas for 30 mins and maintained under a nitrogen atmosphere. Subsequently, the mixture was heated to 70°C. Once temperature equilibration was reached, a mixture of 5.0 g styrene and 0.05 g AIBN was injected dropwise into the reaction flask. The polymerization was allowed to proceed for 24 hours under nitrogen at 300 rpm. A milky white colloidal dispersion was obtained at the end. The dispersion was filtered through glass wool and cleaned via 3 cycles of centrifugation and re-dispersion to obtain a final colloidal dispersion of PEGMA-stabilized polystyrene particles in Millipore water.

2.3. Particle characterisation

2.3.1. Size and electrophoretic mobility measurements

The polystyrene particles were sized by dynamic light scattering using a Zetasizer Nano ZS (Malvern Instruments Ltd). The particles, diluted to 0.02% in 1.5 mL Millipore water or KCl solution, were measured three times at 25°C with each

measurement taken as an average of ten runs. The electrophoretic mobility of the particles was also measured with Zetasizer Nano ZS in a disposable capillary cell. The particles were diluted to 0.02% in 1.0 mL Millipore water or KCl solution. Three measurements were made with each measurement taken as an average of fifty runs. For temperature-dependent sizing and mobility measurements between 25 to 70°C, a temperature increment of 5°C for each measurement was applied and the sample was allowed to equilibrate for 3 mins prior to measurement. For pH-dependent mobility measurements, the samples were measured immediately after pH adjustment.

2.3.2. Scanning electron microscopy (SEM)

50 μ L of 0.2% particle dispersion in ethanol was deposited onto a glass slide, pre-adhered to a SEM stub, and air-dried overnight. The sample was then sputter-coated with platinum at 10 nm thickness in an argon environment. The sample was imaged with Field Emission Gun Scanning Electron Microscope (FEGSEM LEO1530 GEMINI, Carl Zeiss Inc) at 3.0 kV up to 50,000 \times magnification.

2.4. Centrifugal sedimentation

The centrifugal sedimentation experiments were carried out in a LUMiSizer[®] 611 (L.U.M. GmbH). The analytical centrifugation technique is based on the measurement of transmitted light intensity as a function of time and position over the sample length. The particle concentration within the sample is given by the transmission profiles (whereby low concentration is represented by high transmission, and vice versa). 400 μ L of 5.0 vol% colloidal dispersion was transferred into a 2.0 mm optical path length Polycarbonate (PC) disposable cell. Up to 12 samples were analyzed simultaneously after temperature equilibration. The colloidal dispersions were allowed to form an initial packed bed at 1000 rpm ($\sim 145 \times g$) for 8 hours. During this period, the transmission profile was collected every 10 mins. Subsequently the centrifugal field was increased by 500 rpm every 68 mins up to 4000 rpm ($\sim 2325 \times g$), with the transmission profiles collected every 2 mins during the speed ramping.

2.5. Determination of compressive yield stress

2.5.1. At initial condition, $P_y(\phi_0)$

The determination of compressive yield stress, $P_y(\phi)$, is based on the approach of Buscall and White.¹⁵ Under a constant centrifugal field, the particle dispersion is expected to settle over time to form a bed of sediment with defined height. The initial rate of change of the sediment height, dH/dt , is given in Equation 1.^{15,16}

$$\left. \frac{dH}{dt} \right|_0 = -\frac{(1-\phi_0)u_0}{r(\phi_0)} \left(1 - \frac{P_y(\phi_0)}{\Delta\rho g\phi_0 H_0} \right) \quad (1)$$

Where ϕ_0 is the initial (uniform) volume fraction of particle dispersion, $r(\phi_0)$ is the volume fraction dependent hindered settling factor, u_0 is the sedimentation rate of an isolated particle, $P_y(\phi_0)$ is the compressive yield stress when volume fraction of particle dispersion is ϕ_0 , $\Delta\rho$ is the density difference between

particle and liquid, g is the centrifugal acceleration at the bottom of the bed and H_0 is the initial sediment height.

$r(\phi_0)$ accounts for the increase in hydrodynamic interactions between particles with an increase in the particle concentration due to sedimentation, in this case. Increased concentration leads to a deviation from Stokes free settling regime and $r(\phi) \rightarrow 1$ as $\phi \rightarrow 0$ and $r(\phi) \rightarrow \infty$ as $\phi \rightarrow 1$.^{15,16} This means when the particle concentration is low, i.e. $\phi \rightarrow 0$, particles are unaffected by any neighbors and thus $r(\phi) \rightarrow 1$. However, when the particle concentration increases, i.e. $\phi \rightarrow 1$, the settling velocity is affected by hydrodynamic interactions between particles and this results in an exponential increase for $r(\phi)$, i.e. $r(\phi) \rightarrow \infty$. This upper limit is only theoretical, as in practice the maximum achievable close packed concentration is 0.64, which represents the close packing of random monodisperse hard spheres.¹⁶

For an initial particle volume fraction of 0.05, the influence of $(1 - \phi_0)/r(\phi_0)$ is approximated to be of order 1. Hence, it is possible to plot Equation 1, giving a straight line of $-(1/g)(dH/dt)$ against $(\Delta\rho g\phi_0 H_0)^{-1}$ with y-axis intercept I and slope $-IP_y(\phi_0)$. Thus, the initial compressive yield stress, $P_y(\phi_0)$, can be determined. (Further information on simplification of Equation 1 is provided in the Supplementary Information – S1.)

2.5.2. At equilibrium, $P_y(\phi_{eq})$

During the sediment bed preparation stage, whereby a constant centrifugal field is applied for 8 hours at 1000 rpm ($\sim 145g$), the particle dispersion settles over time to form a bed of sediment with defined height. The sediment height is a result of the force balance between the compressive forces (induced by centrifugal acceleration) with the strength of the formed particle network i.e. the compressive yield stress at equilibrium, $P_y(\phi_{eq})$. The sediment height will change with increasing centrifugal acceleration, the amount of change depending on the structure of the particle network and its strength.

Once the particle bed has achieved equilibrium, the compressive yield stress, $P_y(\phi_{eq})$, at each (increasing) applied centrifugation force, can be determined by using the mean value approximation theorem according to Equations 2 and 3.^{15,16}

$$P_y(\phi_{eq}) \approx \Delta\rho g\phi_0 H_0 \left(1 - \frac{H_{eq}}{2L}\right) \quad (2)$$

$$\phi_{eq} \approx \frac{\phi_0 H_0 \left[1 - \frac{1}{2L} \left(H_{eq} + g \frac{dH_{eq}}{dg}\right)\right]}{\left(H_{eq} + g \frac{dH_{eq}}{dg}\right) \left(1 - \frac{H_{eq}}{L}\right) + \frac{H_{eq}^2}{2L}} \quad (3)$$

Where $P_y(\phi_{eq})$ is the compressive yield stress at equilibrium, ϕ_0 and ϕ_{eq} are the initial and equilibrium volume fraction of particle dispersions respectively, $\Delta\rho$ is the density difference between particle and liquid, g is the centrifugal acceleration at the bottom of the bed, H_0 and H_{eq} are the initial and equilibrium sediment heights respectively and L is the radial distance from centrifuge center to bottom of bed. Figure 1 presents a schematic of the experiment setup for centrifugal sedimentation.

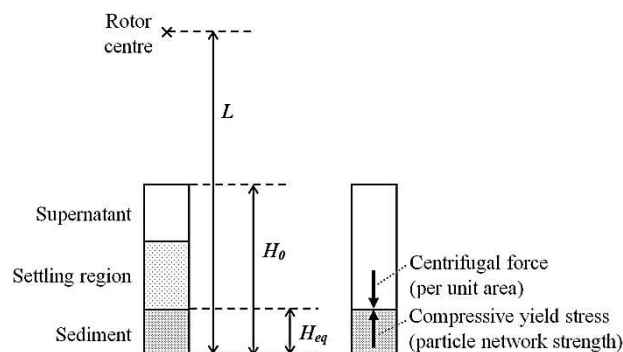


Fig. 1 Schematic for centrifugation sedimentation experiment setup (not according to scale)

3. Results and discussions

3.1. Particle characterisation

Polystyrene particles were successfully synthesized in the presence of a polymeric stabilizer, methoxypolyethylene glycol methacrylate (PEGMA) (MW ~ 2080). The particles were imaged by SEM (Figure 2a) and had a mean size of 816 ± 24 nm (measurement averaged over 100 particles). The PEGMA-stabilized particles were also sized by dynamic light scattering (DLS) as a function of temperature (Figure 2b). These particles demonstrated a temperature-sensitive hydrodynamic diameter, with an average of 880 nm (polydispersity index, PDI ~ 0.06) at 25°C and 820 nm (PDI ~ 0.06) at 60°C when dispersed in Millipore water. The thermal behavior of PEGMA was also observed by Pich *et al.*²⁴ and this characteristic has been utilised by Fu *et al.*²⁵ to synthesise particles from copolymers of diisocyanate and poly(ethylene glycol) (PEG). In both cases, the critical temperature was observed to fall between 25 and 45°C depending on the PEG molecular weight ($526 < \text{MW} < 2000$). This is consistent with our work, where a decrease in PEGMA shell thickness was first observed at around 45°C (Figure 2b). Below 45°C, the polymeric stabilizer is extended into a good solvent providing efficient steric stabilization and stable monodisperse “larger” core/shell particles. Above 45°C, the polymeric stabilizer collapsed towards the particle surface, forming more “hard sphere”-like particles. This is most likely due to reduced polymer solvency as a result of disruption of hydrogen bonding at higher temperatures. As a result of insufficient steric stabilization on particle surface, the onset of particle aggregation was observed at temperatures beyond 60°C, as detected by DLS (Figure 2b).

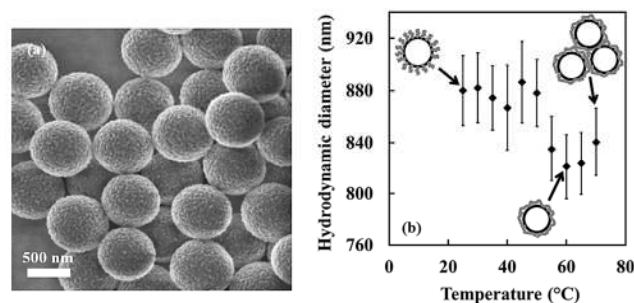


Fig. 2 (a) SEM image of PEGMA-stabilised polystyrene particles and (b) the effect of temperature on the hydrodynamic diameter of these particles, with schematic representations of the particle morphology

3.2. Centrifugal sedimentation

3.2.1. Effect of temperature

Two PC cells were each loaded with 400 μL of 5.0 vol% PEGMA-stabilized polystyrene particle dispersion. Both samples were subjected to an identical speed ramping procedure in the LUMiSizer[®] (1000 rpm for 8 hours to build the particle bed, and subsequently 500 rpm increments every 68 mins up to 4000 rpm): Sample 1 was run at 25°C and Sample 2 at 60°C. The sedimentation results for both samples are presented in Figure 3. Below the critical temperature (T_c) (i.e. at 45°C for the studied particles) (denoted by \times), the sedimentation profile at 25°C showed a gradual height reduction from 22.0 mm (initial uniform dispersion height) to 2.8 mm (packed bed height) within the first 2.5 hours. This sample profile then plateaued at 2.8 mm for the remainder of the experiment, despite incremental increases in the centrifugal field. Above T_c (denoted by +), the sedimentation profile at 60°C showed a dramatic height change of 15.6 mm in the first 40 mins to give a bed height of 6.4 mm. Subsequently, the sediment bed was compressed further by incremental increases of the applied centrifugal field, to give a final packed bed height of 4.5 mm at 4000 rpm.

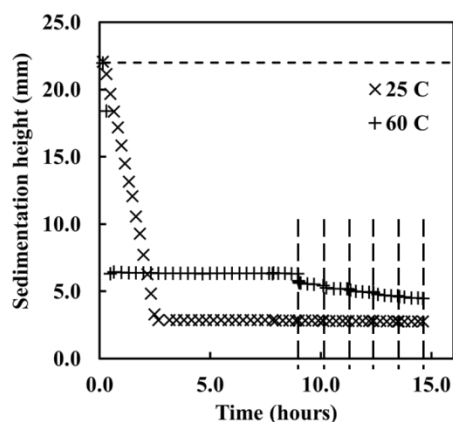


Fig. 3 Sedimentation profiles for PEGMA-polystyrene particles at temperatures below (Sample 1 – 25°C) and above (Sample 2 – 60°C) the critical temperature (T_c) (vertical dash lines corresponds to increment in centrifugal field strength)

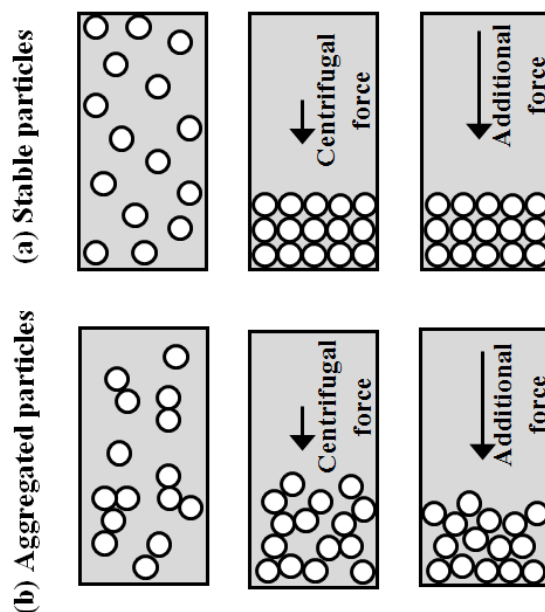


Fig. 4 Schematic diagram for the effect of centrifugal field on the sedimentation of (a) stable particles and (b) aggregates

These observations can be explained by the stability behavior of PEGMA-stabilized particles, as depicted schematically in Figure 4. Below T_c , the polystyrene particles are sterically stabilized by the presence of extended PEGMA stabilizers on the particle surface. Under this condition, as the centrifugal field is applied, the individual particles gradually settle over time and are able to arrange into a very close packed bed (Figure 4a). Subsequently, as the centrifugal field is increased over time, the particles, which are already in a strongly close packing arrangement, are prevented from further particle rearrangement. Hence, any additional centrifugal force is unable to compress the particle bed further. In contrast, above T_c , the solvency of PEGMA stabilizers is compromised, resulting in instability of the polystyrene particles and aggregation into larger structures (Figure 2b). Under these conditions, the aggregated polystyrene particles initially form a more open particle bed structure under the applied centrifugal field (Figure 3b). These larger mass aggregates, when compared to stable individual particles, settle faster, leading to shorter sediment bed formation time, as seen in Figure 3 (Sample 2). Subsequently, as larger centrifugal forces are applied to the particle bed, the initially more open structure allows the particles to rearrange under the applied force, resulting in a partial collapse of the structure and a compaction of the settled bed. Hence, a stepwise profile is obtained for the sediment bed height as a function of the applied centrifugal force, depicted in the data for Sample 2 (Figure 3). The observed particle packing behavior with respect to applied centrifugal force is consistent with other research,^{26,27,28} whereby stable particle dispersions form a pressure-insensitive packed bed while aggregated particles have pressure-dependent network.

3.2.2. Effect of electrolyte addition

It has been shown previously via various techniques, including cloud point measurements,^{29,30,31} rheology,^{32,33} and NMR,³⁴ that the solvency of poly(ethylene glycol) (PEG) chains in water can

be compromised by the addition of electrolyte. The addition of electrolyte has two effects on the PEG polymeric chains; firstly it disrupts the hydrogen bonding between the ether groups and water molecules and secondly it binds to the PEG thus screening the weak electrostatics induced by the ion-dipole interactions around the oxygen atoms on the polymer chains.³⁵ Hence, when electrolyte, in this case potassium chloride (KCl), was added to the PEGMA-stabilized polystyrene particle dispersions, it was possible to detect the effect of KCl addition on the dispersion

stability using the LUMiSizer[®] measurements. The results for the addition of KCl to the particle dispersions under conditions below and above the T_c are illustrated in Figure 5.

Figure 5a depicts the effect of KCl on the stability of polystyrene particle dispersions at 25°C. It can be seen immediately that the addition of electrolyte induces particle aggregation, as evidenced by the stepwise profiles and the substantial sedimentation within the first hour when compared to

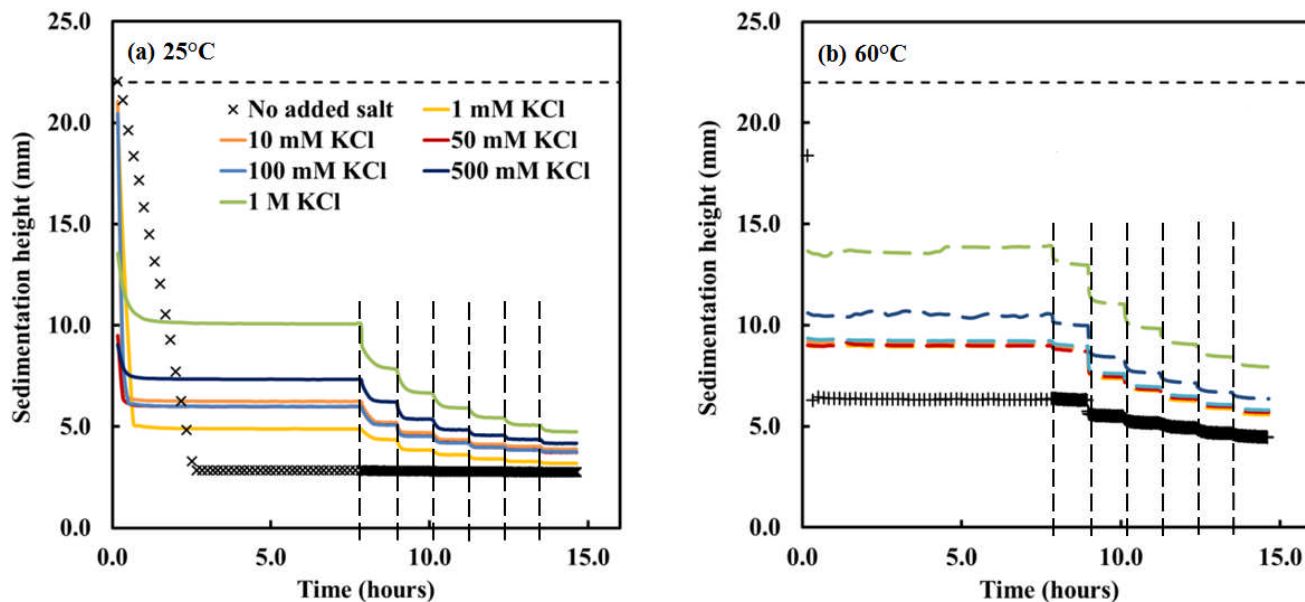


Fig. 5 Effect of electrolyte concentration on the sedimentation of 5 vol% PEGMA-stabilized polystyrene particle dispersion at (a) 25°C and (b) 60°C (vertical dash lines corresponds to increment in centrifugal field strength) (Legend applicable for both graphs; Symbol – ‘no added salt’ dataset at respective temperature, Coloured lines – dataset at increasing KCl concentration)

the gradual height change over 2.5 hours seen for the stable particle dispersion (i.e. no added salt). The extent of particle aggregation is seen to increase with increasing KCl concentrations, as inferred from the initial equilibrium sediment height of 5.0 mm in 1 mM KCl solution up to 10.2 mm in 1 M KCl solution. The general increase in sediment height, as a function of the added electrolyte concentration, is attributed to the greater dehydration of the PEG chains and/or the double-layer screening effects on the colloids as more KCl ions are added to the system. Both effects can drive the formation of larger aggregates as the salt concentration is increased, which produces correspondingly less compact sediment beds. Ultimately, this is linked to an increase in the depth of the attractive interaction minimum with increasing electrolyte, affecting the particle aggregation rate and size/density of aggregates formed.^{7,36}

Further increases in the applied centrifugal field at increments of 500 rpm up to a final speed of 4000 rpm showed a characteristic collapse profile of the sediment beds with the degree of collapse for these beds increasing with increased electrolyte concentrations (~ 1.8 mm at 1 mM KCl up to ~ 5.4 mm at 1 M KCl). The more open bed structure at 1 M KCl clearly allows greater flexibility for the particles to rearrange and exclude the supernatant volume, hence leading to larger particle bed compression. This is in agreement with Florin *et al.*²⁹ and Anathapadmanabhan and Goddard,³⁰ who have previously

demonstrated an enhanced phase separation of PEG chains from water/KCl system at high electrolyte concentrations.

Interestingly, in Figure 5a, it was seen that the sedimentation behavior for particles dispersed in 10, 50 and 100 mM KCl solutions were almost identical. This is perhaps indicative of the changes in two separate, but linked, interactions as the electrolyte concentration is increased. The PEGMA-stabilized colloidal particles are expected to have a short-range steric layer induced by the polymeric shell. They are also expected to have some residual surface charge from the synthetic procedure, which will result in the formation of an electric double layer around the particles. The surface charge was found to be negative by electrophoretic mobility measurements, as shown in Figure 6. Yamamoto reported similar negatively charged polystyrene particles when the synthesis used AIBN in water, whereby the charge was attributed to the localized pi electron cloud of the benzene ring in the monomer.³⁷

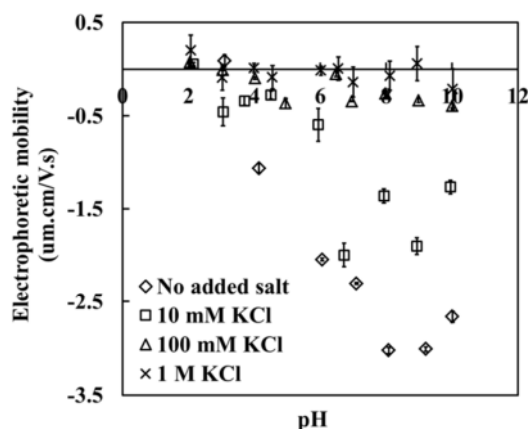


Fig. 6 Effect of electrolyte concentration on the electrophoretic mobility of PEGMA-stabilized polystyrene particles at 25°C

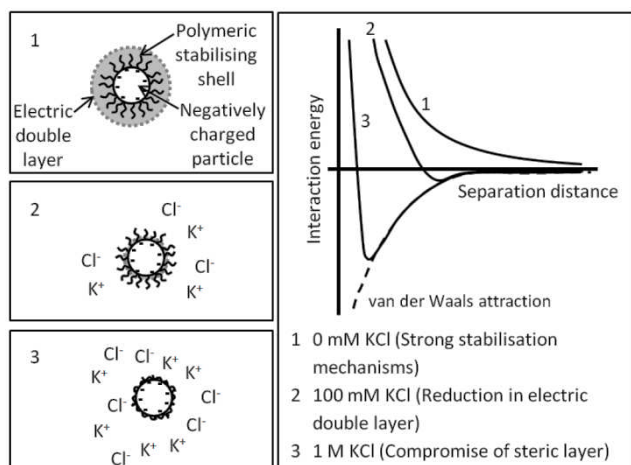


Fig. 7 Schematic diagram of the effect of electrolyte concentration on the stabilization mechanisms of PEGMA-stabilized polystyrene particles

At low salt levels, the double layer may be expected to extend beyond the steric layer providing a strong additional stabilization mechanism for these particles. As the electrolyte level increases, the double layer extent will decrease. It is postulated here that below 100 mM KCl, weak particle aggregation occurs within a secondary minimum, as the particles retain sufficient steric stabilization from the PEGMA chains. This is in agreement with the electrophoretic mobility measurements (Figure 6), which show an essentially zero value at 100 mM KCl and above. At higher salt levels, the steric layer of the PEGMA shell is, in turn, strongly compromised. The polymeric chains are now increasingly dehydrated, resulting in the collapse of the polymer back to the particle surface. This creates a progressively deeper interaction minimum that induces further particle aggregation. Figure 7 schematically summarizes the effect of electrolyte concentration on the stabilization mechanisms of the PEGMA-stabilized polystyrene particles.

Figure 5b gives a corresponding set of sedimentation profiles for PEGMA-stabilized polystyrene particles at similar electrolyte concentrations, but now at the higher temperature of 60°C. Overall, the sedimentation behaviour at 60°C was similar to that seen at 25°C, with the exception that the dehydrated PEGMA chains, as a result of temperature elevation, had now compromised the steric stabilization of the particles. This resulted

in a greater degree of particle aggregation, leading to more voluminous particle beds for all electrolyte concentrations. These sedimentation data are in agreement with DLS size measurements (Figure 8), which were measured as a function of temperature and KCl concentration. Under a salt-free condition, the PEGMA-stabilized particles were stable below T_c with a measured size of ~880 nm. These particles subsequently showed shrinkage in the polymeric shell to ~820 nm at 60°C. These data, previously given in Figure 2b, form the baseline here for the data with added electrolyte. In 10 and 100 mM KCl solutions, the sizing results were similar, with some indication of particle aggregation at higher temperatures. In 1 M KCl, the particles aggregated significantly to sizes of over 1 μm for temperatures beyond 40°C. It is worth pointing out that the extent of particle aggregation seen in DLS measurements will be limited due to the measurements being made at dilute particle concentration of 0.02 vol%, as opposed to LUMiSizer® sedimentation experiments at 5 vol%.

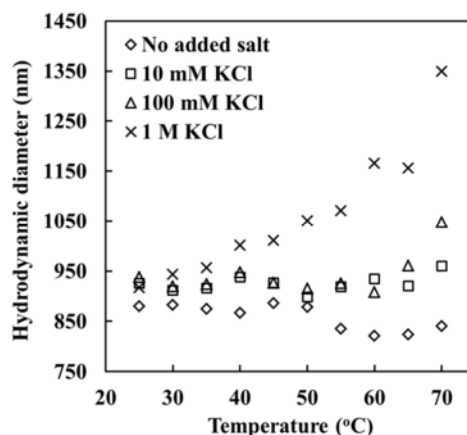


Fig. 8 Effect of electrolyte concentration on the particle size of PEGMA-stabilized polystyrene particles as a function of temperature

3.3. Compressive yield stress data

According to Buscall and White,¹⁵ the application of an external force onto the particle bed causes the bed to compress to a new equilibrium height, where the particle bed acquires adequate strength to balance the applied force. During this process, the particles rearrange into a closer packed structure and the liquid is squeezed from the interstices forming a stronger particle network. The particle network strength can be characterized by the compressive yield stress, $P_y(\phi)$, and typically this is dependent on the shear history during aggregation, the strength of inter-particle interaction forces and the local volume concentration of particles.^{9,15} For this work, the particle dispersions were treated identically, whereby KCl solutions of desired concentration were added to a particle dispersion, shaken for 30 seconds and then pipetted into the LUMiSizer® cell. Hence, the effect of shear history on $P_y(\phi)$ was negligible.

3.3.1. At equilibrium, $P_y(\phi_{eq})$

As observed from Figure 5, the aggregated sediment beds, in increasing KCl concentrations, exhibited different compression

responses despite being subjected to identical centrifugal forces. This is also illustrated in Figure 9, which plots the equilibrium sediment height, H_{eq} , at each applied centrifugal force, g , for both 25 and 60°C. In Figure 9a, with no added KCl at 25°C, H_{eq} remained constant irrespective of the applied acceleration, indicating a close-packed bed of stable particles had been formed. With increasing electrolyte concentration, the H_{eq} data followed a natural logarithmic fitting ($0.95 < R^2 \text{ value} < 0.97$, data shown in Supplementary Information – S2,) with H_{eq} decreasing rapidly at low acceleration and eventually reaching a plateau at high acceleration values. An increased in KCl concentration led to more voluminous sediment beds with a correspondingly larger compressive behavior. At 60°C (Figure 9b), the change in H_{eq} also follows a natural logarithmic fitting for all experimental conditions (data shown in Supplementary Information – S2). Due to the high temperature, the steric stabilizing shell was

compromised; this resulted in particle aggregation and thus changes to the sediment height, even in the case of no added electrolyte.

The equilibrium volume fraction of particles, ϕ_{eq} , and compressive yield stress, $P_y(\phi_{eq})$, at each centrifugation stage can be determined using Figure 9 together with Equations 2 and 3.^{15,16} Figure 10 presents the compressibility of the particle networks, as a plot of $P_y(\phi_{eq})$ with the corresponding ϕ_{eq} , as a function of electrolyte concentration for both temperatures (symbols representing the experimental datasets, dashed lines are power-law fits). From Figure 10a, it is observed that, at 25°C, for a low electrolyte concentration (i.e. 1 mM KCl), the particle network initially formed the most densely packed bed at low pressures and experienced a much smaller overall compression at

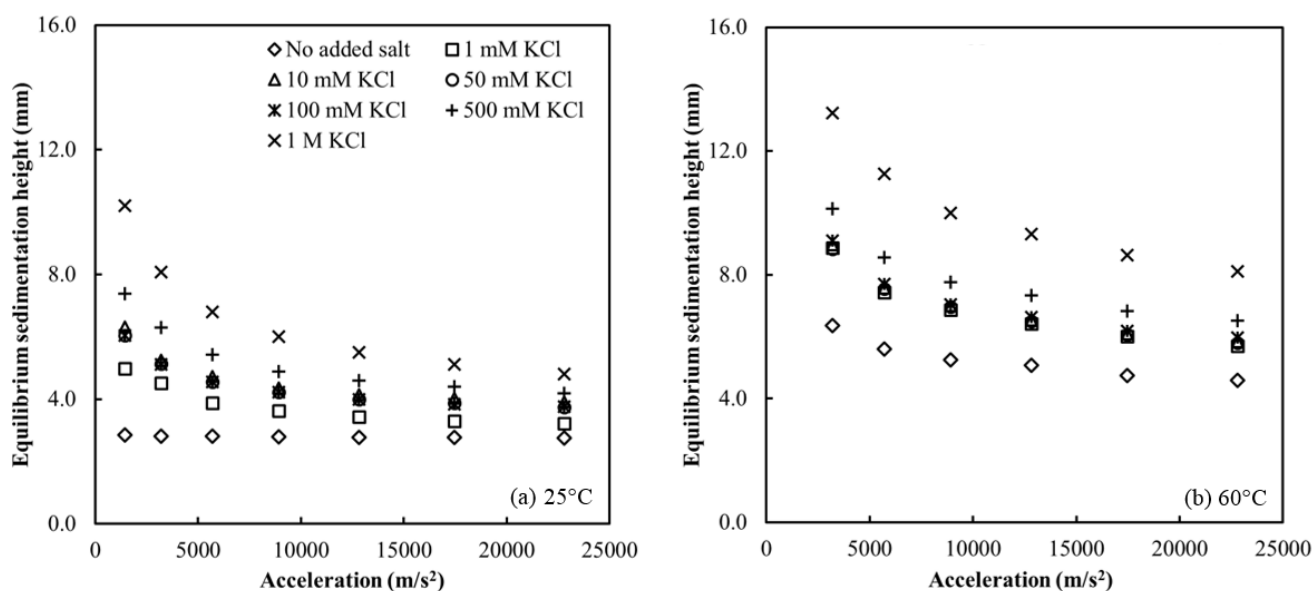


Fig. 9 Equilibrium sedimentation height as a function of acceleration for 5 vol% PEGMA-stabilized polystyrene particle dispersions at varying electrolyte concentrations (a) 25°C and (b) 60°C (Legend applicable for both graphs)

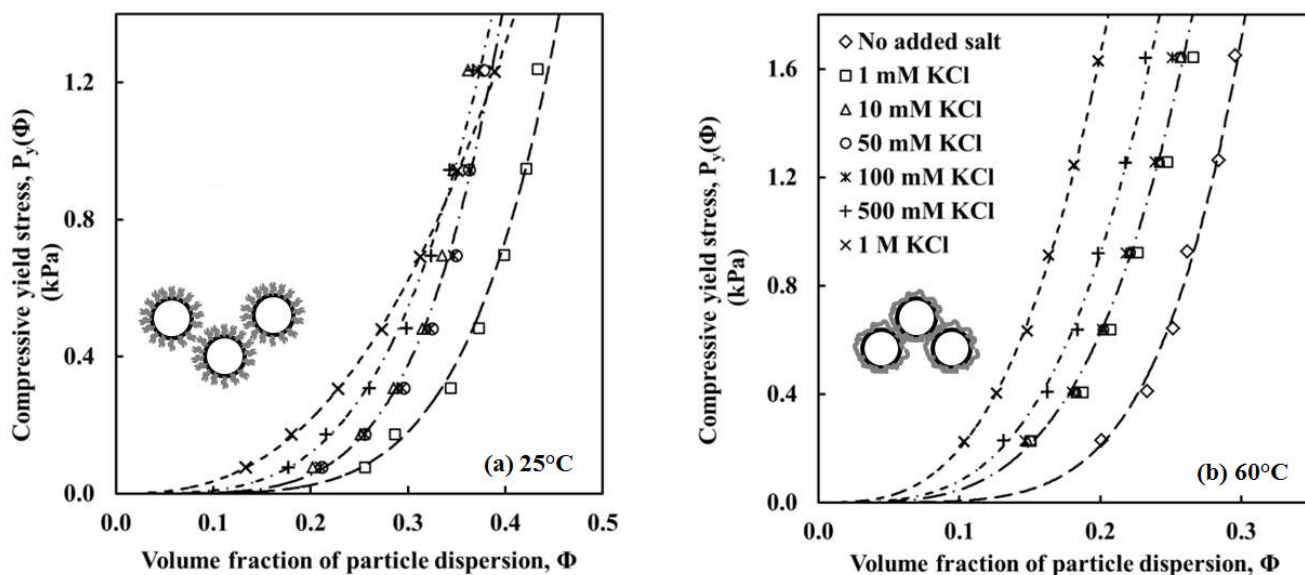


Fig. 10 Compressive yield stress, $P_y(\phi_{eq})$, at equilibrium as determined by mean value approximation for 5 vol% PEGMA-stabilized polystyrene particle dispersion at varying electrolyte concentrations for (a) 25°C and (b) 60°C (Legend applicable for both graphs; Symbol – dataset at respective KCl concentration; Dashed line – corresponding power-law fit; Schematics – ‘sterically repulsive’ solvated shell structure at 25°C and ‘sterically-attractive’ collapsed polymers at 60°C) (Please note that there are no diamond symbols in Fig. 10(a) as compressive yield stress can only be determined for unstable dispersions and this is not applicable to stable PEGMA-stabilized polystyrene particles at 25°C with no added salt.)

higher pressures. With an increase in electrolyte concentration, the particle networks generally exhibited an increased level of compression under the applied force. This is the result of larger aggregates being formed at higher KCl concentrations (detected by DLS at 25°C in Figure 8), thus giving correspondingly less dense particle beds initially. However, presumably due to the presence of a ‘soft, flexible’ steric polymer shell at 25°C, the applied centrifugal force was able to compress the particle beds to almost an identical volume fraction under maximum centrifugal field (~ 2325 $\times g$) (for 10 mM to 1 M KCl). It is worth pointing out that for Figure 10, the ϕ_{eq} corresponds to the volume fraction of particles at the bottom of the cell. This will be different from the volume fraction of particles at the sediment/supernatant interface as the applied centrifugal force is a function of distance from the centrifuge center (i.e. axis of rotation).

The general form of the compressibility data at 60°C (Figure 10b) is similar to that at 25°C, with the particle networks formed at lower electrolyte concentrations exhibiting initially higher packing density at low compressions. In this case, however, the absolute degree of compressibility at different electrolyte concentrations is not seen to change significantly as the electrolyte concentration rises. This is attributed to the generally stronger inter-particle interactions at all electrolyte concentrations, when compared with those at the lower temperature, a result of the collapse of the stabilizing steric layer at 60°C (above the critical temperature, T_c). In addition to van der Waals attraction, it has been proposed that the poorly soluble polymeric stabilizers on the particle surface induce an additional ‘hydrophobic’ attraction. The ‘hydrophobic’ attraction was first presented by Klein,^{38,39} who observed the presence of an attractive force in a poor organic solvent for two approaching polymeric coated surfaces. This observation was also seen recently by the Franks group⁴⁰ during their temperature investigation of the hydrophilic/hydrophobic nature of poly(N-

isopropylacrylamide) (PNIPAM) in order to manipulate inter-particle interactions. The van der Waals forces and longer range (up to 50 nm) ‘hydrophobic’ attractions allow for stronger adhesion bonds between the particle-particle contacts. This renders them difficult to be broken for particle rearrangement and bed compaction to occur even though the degree of compression is increased. Hence, the particle networks, at all electrolyte concentrations, are better able to withstand the applied centrifugal field.

At temperatures below T_c (i.e. at 25°C), these PEGMA-stabilized polystyrene particles possess a ‘sterically-repulsive’ solvated shell that allows the compression of the polymeric shell when the system is under high compression. While at temperatures above T_c (i.e. at 60°C), the particles have an ‘attractive’ collapsed polymer layer on the particle surface with strong inter-particle attractions that do not allow for further compressions. The particle structures at both temperatures are schematically represented in the respective insets to Figure 10.

3.3.2. At initial condition, $P_y(\phi_0)$

The role of the steric polymer layer is further supported by the analysis of the compressive yield stress data at initial conditions, $P_y(\phi_0)$, shown in Figure 11. Please note that the initial conditions in this work represent the starting uniform volume fraction for the particle dispersions just before sedimentation takes place. For this work, the initial volume fraction, ϕ_0 , is 5 vol%. At 25°C, $P_y(\phi_0)$ is seen to decrease with KCl concentration, while at 60°C, $P_y(\phi_0)$ remains constant throughout. This data trend is consistent with a change in the inter-particle interactions between the particles when under compression. Below T_c , PEGMA stabilizers are expected to be hydrated and extended at low electrolyte conditions (e.g. 1 mM KCl). This produces strongly sterically-stabilized particles

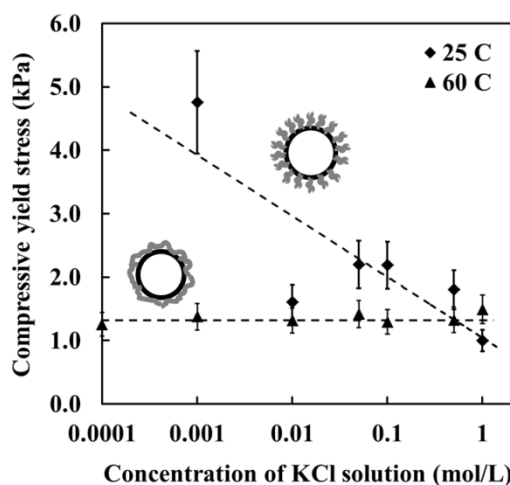


Fig. 11 Compressive yield stress, $P_y(\phi_o)$, under initial (uniform) conditions for PEGMA-stabilized polystyrene particle dispersions as a function of electrolyte concentration at 25 and 60°C. Schematics of particle structure presented for respective temperature of 25 and 60°C. (Dashed lines as guide to eye)

with good stability. Hence, larger pressure, or an equivalently longer centrifugal duration, is necessary to force the particles into closer contact, translating to a greater compressive yield stress at initial condition. With increasing electrolyte concentrations, the PEGMA shell is gradually compromised due to poor solvency of the polymers. Under these conditions, the electro-steric repulsion between the polystyrene particles is weakened, allowing the particles to approach one another more easily. This means a smaller compression force is required, leading to a smaller initial compressive yield stress, $P_y(\phi_o)$. Above T_c , the PEGMA polymers are dehydrated due to disruption in hydrogen bonding between the polymers and water molecules. This thus compromises the steric stabilization layer, whereby under these conditions, the inter-particle interactions are dominated by attractive forces (i.e. van der Waals and 'hydrophobic' attractions), which are effective when the particles are close enough to each other. Therefore, the particles are able to approach each other easily, giving a more consistent compressive yield stress, $P_y(\phi_o)$. The force required to bring the particles close together should be identical for all electrolyte concentrations under high temperatures. The observed trend for $P_y(\phi_o)$ is consistent to the sedimentation behavior in Figure 5 during the particle bed preparation at 1000 rpm (i.e. within the first 8 hours). It is worth pointing out that $P_y(\phi_o)$ is an indicator for the sedimentation behavior of the colloidal dispersions. This takes into account the hindered settling effect, which is dependent on the hydrodynamic drag and total volume fraction of the particle dispersion. It does not represent the particle network strength for sedimented beds as this is also governed by the shear history during aggregation, strength of inter-particle interaction forces and local volume concentration of particles.

3.3.3. Average packing density of particle beds, ϕ_m

An alternative method to characterize the overall compression of the particle networks is from the average packing density of the

particle bed for a given applied pressure. In Figure 12, the average packing density, ϕ_m , against the excess pressure at the bottom of the particle bed, P_b , is given. These data confirm the sediment densification observations from Figure 5 for the different electrolyte concentrations, at both 25 and 60°C. The average packing density, ϕ_m , and the excess pressure at the bottom of the bed, P_b , are calculated according to Equations 4 and 5 respectively.⁹

$$\phi_m = \frac{m_s}{\rho_s V} \quad (4)$$

$$P_b = \frac{\Delta\rho L}{\rho_s A} \omega^2 m_s \quad (5)$$

Where m_s is the mass of particles in sediment, ρ_s is the density of particles, V is the sediment volume deduced from the position of sediment/supernatant interface, $\Delta\rho$ is the density difference between particle and liquid, L is the radial distance from centrifuge center to bottom of bed, A is the cross-sectional area of sediment at bottom of bed and ω is the angular velocity.

For stable particles with no added electrolyte at 25°C (Figure 12a, diamond symbols), the dispersion exhibits a dense packing at low pressure with minimal compression at higher pressures. These data also show how the aggregated dispersions, due to the presence of electrolyte, initially reach a low packing density before gradually being consolidated by up to 110% at higher pressures. Similar consolidation behaviour is also observed for the aggregated particles at 60°C (Figure 12b), but with a smaller degree of bed compression (~39%) due to the stronger attraction forces, and thus adhesion bonding at the particle-particle contacts at 60°C. The average packing density, ϕ_m , calculation (Figure 12) is found to be complimentary to the equilibrium volume fraction of particles, ϕ_{eq} , (Figure 11), particularly at low centrifugal fields for 25°C and for all centrifugal fields at 60°C. This supports the compressive rheology behaviour for PEGMA-stabilized polystyrene particles in varying electrolyte concentrations for both temperatures below and above T_c . It is worth pointing out that Equation 4 refers to the average packing density of hard particles. Thus, this does not truly describe the average packing density for sterically-stabilized particles in Figure 12a, particularly when the PEGMA shells are fully extended. The total volume (i.e. particle core + extended polymeric shell) should be considered in the determination of average packing density for sterically-stabilised particles. The trend in Figure 12a remains valid as the effect of shell volume diminishes with increasing electrolyte concentration. Based on numerical calculations, which accounts for shell volume contribution, the average packing density for this configuration of stable PEGMA-stabilized polystyrene particles at 25°C with no added electrolyte is found to be ~ 52%. This is equivalent to closed packed bed in simple cubic arrangement.

Cite this: DOI: 10.1039/c0xx00000x

www.rsc.org/xxxxxx

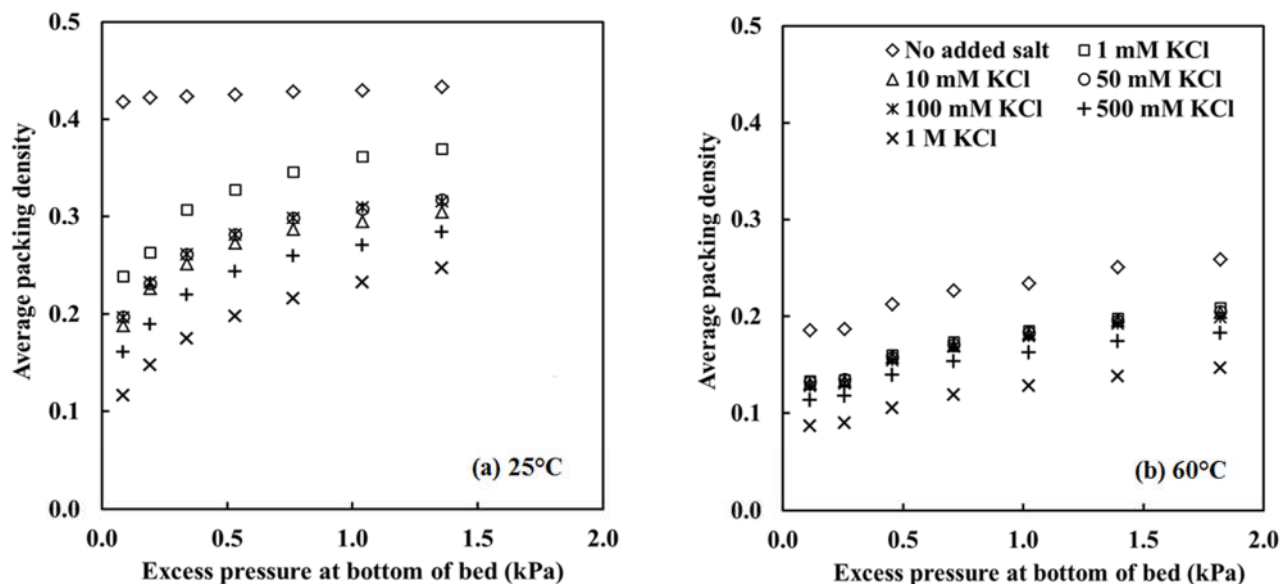


Fig. 12 Comparison of compressive properties for PEGMA-stabilized polystyrene particle dispersions in different electrolyte concentrations at (a) 25 and (b) 60°C (Legend applicable for both graphs)

4. Conclusions

5 An analytical centrifugation technique was used to investigate the sedimentation behaviour of sterically-stabilized temperature-sensitive colloidal particles, in this case methoxy poly(ethylene glycol) methacrylate (PEGMA)-stabilized polystyrene (PS) particles. The colloidal stability of PEGMA-PS particles was investigated as a function of temperature and electrolyte concentration. Two types of sedimentation profiles were obtained; (i) smooth constant profile which remained unchanged with increasing centrifugal force for stable particle dispersions and (ii) stepwise profile which compressed with increasing force for aggregated dispersions. The sedimentation profiles showed the extent of particle aggregation as a function of electrolyte concentration, with more prominent effect at higher temperatures due to dehydration of PEGMA polymeric chains at 60°C, which induced greater instability in the PEGMA-PS particle dispersion.

20 Upon formation of sediment beds, the equilibrium compressive yield stress, $P_y(\phi_{eq})$, showed a power-law dependency on the volume fraction of particles, with denser particle bed required to withstand the same centrifugal force when the particle network is formed at low electrolyte concentrations. This was due to larger aggregates and stronger inter-particle interactions at higher electrolyte concentrations, thus forming more voluminous particle networks. It was also observed that the conformation of the polymeric shell layer, which determined the particle structure (i.e. 'sterically-repulsive' solvated polymeric shell or 'sterically-attractive' collapsed shell), affected the bed compressibility. In

this case, PEGMA, with MW ~ 2080 g/mol, showed a decrease in polymer extension around 45°C, denoted as the critical temperature, T_c , for this work. Below T_c , the flexible solvated shell allowed further compression of the particle bed that eventually led to a fixed value for the final volume fraction of particles at the bottom of the bed. Meanwhile, above T_c , the strong inter-particle attractions and thus adhesion bonds at particle-particle contacts, as a result of the collapse of stabilizing shell layer at higher temperatures, prevented further bed compression.

This particle structure observation was also in agreement with the initial compressive yield stresses, $P_y(\phi_0)$, for the particle networks, which revealed differences in particle network strength at different dispersion conditions. Below T_c , for a uniform dispersion, $P_y(\phi_0)$ highlighted a dependence on the inter-particle interactions of the steric stabilization layer, with greater compression pressure required at low electrolyte conditions. Above T_c , constant $P_y(\phi_0)$ was obtained across electrolyte concentrations for the 'attractive' particles that prefer to be in close proximity to each other. Hence, for a given electrolyte concentration, a corresponding volume fraction of particles was able to withstand the same applied centrifugal field. The sedimentation profiles and compressibility behaviour of the particle beds were also in agreement with the average packing density results.

Symbols

$\Delta\rho$ Density difference between particle and liquid

ρ_s	Density of particles
ϕ_0	Initial (uniform) volume fraction of particle dispersion
ϕ_{eq}	Equilibrium volume fraction of particle dispersion
ϕ_m	Average packing density
5 ω	Angular velocity
A	Cross-sectional area of sediment at bottom of bed
g	Centrifugal acceleration at bottom of bed
H_0	Initial sediment height
H_{eq}	Equilibrium sediment height
10 I	y-axis intercept
L	Radial distance from centrifuge center to bottom of bed
MW	Molecular weight of polymer
m_s	Mass of particles in the sediment
P_b	Excess pressure at the bottom of bed
15 $P_y(\phi_0)$	Compressive yield stress for ϕ_0
$P_y(\phi_{eq})$	Compressive yield stress at equilibrium
$r(\phi_0)$	Dimensionless hydrodynamic interaction parameter
T_c	Critical temperature
u_0	Sedimentation rate of an isolated particle
20 V	Sediment volume deduced from position of sediment/supernatant interface

Acknowledgements

This work was financially supported by EPSRC under the project grant of 'Innovation in Industrial Inkjet Technology' (EP/H018913/1). The authors would like to thank Dr Anthony Stickland for the helpful discussions and to IMCD UK Ltd for their kind donation of polymeric stabilizer, methoxypolyethylene glycol methacrylate (PEGMA).

Notes and references

³⁰ ^a University of Leeds, Institute of Particle Science and Engineering, School of Process, Environmental and Materials Engineering, Leeds LS2 9JT, United Kingdom. E-mail: h.n.yow@leeds.ac.uk

- R. J. Hunter, *Foundations of Colloid Science*, 2nd ed, Oxford University Press, Oxford, UK, 2001.
- T. Cosgrove T (ed), *Colloid Science: Principles, Methods and Applications*, John Wiley & Sons Ltd, Chichester, UK, 2010.
- S. Xu and Z. Sun, *Soft Matter*, 2011, **7**, 11298-11308.
- J. Gregory, *Adv. Colloid Interface Sci.*, 2009, **147-148**, 109-123.
- G. V. Franks, *J. Colloid Interface Sci.*, 2005, **292**, 598-603.
- G. V. Franks, Y. Zhou, Y. D. Yan, G. J. Jameson and S. Biggs, *Phys. Chem. Chem. Phys.*, 2004, **6**, 4490-4498.
- J. L. Burns, Y. D. Yan, G. J. Jameson and S. Biggs S, *Langmuir*, 1997, **13**, 6413-6420.
- J. N. Smith, J. Meadows and P. A. Williams, *Langmuir*, 1996, **12**, 3773-3778.
- D. Lerche and T. Sobisch, *Powder Tech.*, 2007, **174**, 46-49.
- T. Sobisch and D. Lerche, *Colloid Surf. A*, 2008, **331**, 114-118.
- G. Petzold, C. Goltzsche, M. Mende, S. Schwarz and W. Jaeger, *J. Appl. Polym. Sci.*, 2009, **114**, 696-704.
- H. T. Chiu, C. Y. Chang, T. Y. Chiang, M. T. Kuo and Y. H. Wang, *J. Polym. Sci.*, 2011, **18**, 1587-1596.
- H. T. Chiu, T. Y. Chiang, Y. C. Huang, C. Y. Chang and M. T. Kuo, *Polym-Plast. Technol.*, 2010, **49**, 1552-1562.
- R. Buscall, *Colloid Surf.*, 1982, **5**, 269-283.
- R. Buscall and L. R. White, *J. Chem. Soc. Faraday Trans 1*, 1987, **83**, 873-891.
- R. G. de Krester, D. V. Boger and P. J. Scales, *Rheol. Rev.*, 2003, 125-165.
- R. Buscall, I. J. McGowan, P. D. A. Mills, R. F. Stewart, D. Sutton, L. R. White and G. E. Yates, *J. Non-Newton. Fluid Mech.*, 1987, **24**, 183-202.
- R. Buscall, P. D. A. Mills, J. W. Goodwin and D. W. Lawson, *J. Chem Soc. Faraday Trans. 1*, 1988, **84**, 4249-4260.
- M. D. Green and D. V. Boger, *Ind. Eng. Chem. Res.*, 1997, **69**, 4984-4992.
- W. F. Eckert, J. H. Masliyah, M. R. Gray and P. M. Fedorak, *AIChE J.*, 1996, **42**, 960-972.
- C. E. Colwell and S. M. Livengood, *J. Soc. Cosmet. Chem.*, 1962, **13**, 201-213.
- G. Karlström, A. Carlsson and B. Lindman, *J. Phys. Chem.*, 1990, **94**, 5005-5015.
- S. Fujii, P. D. Iddon, A. J. Ryan and S. P. Armes, *Langmuir*, 2006, **22**, 7512-7520.
- A. Pich, Y. Lu and H. J. Adler, *Colloid Polym. Sci.*, 2003, **281**, 907-915.
- H. Fu, H. Gao, G. Wu, Y. Wang, Y. Fan and J. Ma, *Soft Matter*, 2011, **7**, 3546-3552.
- F. F. Lange and K. T. Miller, *Am. Ceram. Soc. Bull.*, 1987, **66**, 1498-1504.
- J. C. Chang, F. F. Lange and D. S. Pearson, *J. Am. Ceram. Soc.*, 1994, **77**, 1357-1360.
- L. Bergström, C. H. Schilling and I. A. Aksay, *J. Am. Ceram. Soc.*, 1992, **75**, 3305-3314.
- E. Florin, R. Kjellander and J. C. Eriksson, *J. Chem. Soc. Faraday Trans. 1*, 1984, **80**, 2889-2910.
- K. P. Ananthapadmanabhan and E. D. Goddard, *Langmuir*, 1987, **3**, 25-31.
- M. Dilip, S. T. Griffin, S. K. Spear, H. Rodriguez, C. Rijksen and R. D. Rogers, *Ind. Eng. Chem. Res.*, 2010, **49**, 2371-2379.
- B. Briscoe, P. Luckham and S. Zhu, *Macromolecules*, 1996, **29**, 6208-6211.
- R. D. Lundberg, F. Bailey and R. W. Callard, *J. Polym. Sci. Part A.*, 1966, **4**, 1563-1577.
- M. Björling, G. Karlström and P. Linse, *J. Phys. Chem.*, 1991, **95**, 6706-6709.
- B. Briscoe, P. Luckham and S. Zhu, *Proc. R. Soc. Lond. A*, 1999, **455**, 737-756.
- S. Biggs, *KONA*, 2006, **24**, 41-53.
- T. Yamamoto, *Colloid Polym. Sci.*, 2012, **290**, 1023-1031.
- H. Li, J.-P. O'Shea and G. V. Franks, *AIChE J.*, 2009, **55**, 2070-2080.
- J. Klein, *Adv. Colloid Interface Sci.*, 1982, **16**, 101-115.
- E. Burduková, H. Li, N. Ishida, J.-P. O'Shea and G. V. Franks, *J. Colloid Interface Sci.*, 2010, **342**, 586-592.